Depolarization in Ice Crystals and Its Effect on Radar Polarimetric Measurements

ALEXANDER V. RYZHKOV

Cooperative Institute for Mesoscale Meteorological Studies, University of Oklahoma, and NOAA/OAR/National Severe Storms Laboratory, Norman, Oklahoma

DUSAN S. ZRNIĆ

National Severe Storms Laboratory, Norman, Oklahoma

(Manuscript received 19 July 2006, in final form 12 October 2006)

ABSTRACT

Simultaneous transmission and reception of horizontally and vertically polarized waves is a preferable choice technique for dual-polarization weather radar. One of the consequences of such a choice is possible cross-coupling between orthogonally polarized waves. Cross-coupling depends on depolarizing properties of propagation media, and it is usually negligible in rain because the net mean canting angle of raindrops is close to zero.

Snow crystals at the tops of thunderstorm clouds are often canted in the presence of strong electric fields and produce noticeable cross-coupling between radar signals at horizontal and vertical polarizations if both signals are transmitted and received simultaneously. As a result, peculiar-looking radial signatures of differential reflectivity Z_{DR} and differential phase Φ_{DP} are commonly observed in the crystal regions of thunderstorms.

The paper presents examples of strong depolarization in oriented crystals from the data collected by the polarimetric prototype of the Weather Surveillance Radar-1988 Doppler (WSR-88D) and a theoretical model that explains the results of measurements. It is shown that the sign and magnitude of the Z_{DR} and Φ_{DP} signatures strongly depend on the orientation of crystals and a system differential phase on transmission.

1. Introduction

Simultaneous transmission and reception of horizontally and vertically polarized waves (SHV scheme hereafter) is a preferable choice technique for dual-polarization weather radar (Doviak et al. 2000; Scott et al. 2001). One of the consequences of such a choice is possible cross-coupling between orthogonally polarized waves. Cross-coupling depends on depolarizing properties of propagation media, and it is usually negligible in rain because the net mean canting angle of raindrops is close to zero (Doviak et al. 2000; Ryzhkov et al. 2002; Hubbert and Bringi 2003; Wang et al. 2006).

Snow crystals at the tops of thunderstorm clouds are often canted in the presence of strong electrostatic fields. The effects of crystal orientation in electrically charged zones were studied with polarimetric radars having circular (e.g., Hendry and McCormick 1976; Krehbiel et al. 1996) and linear polarizations (e.g., Caylor and Chandrasekar 1996; Metcalf 1997). These studies showed that pristine crystals with low inertia tend to align along the direction of electrostatic field that generally does not coincide with either horizontal or vertical. After a lightning strike occurs, the magnitude of electric field abruptly diminishes and crystals lose their preferred orientation. They may restore a high degree of common alignment afterward in the case of another build-up of charge or acquire their typical orientation in the absence of electric activity, that is, with larger dimension in the horizontal plane.

If the mean geometrical projection of crystals onto vertical direction is larger than on horizontal direction, then differential phase Φ_{DP} decreases with slant range in the case of alternate transmission and reception, and the corresponding specific differential phase K_{DP} is negative (Caylor and Chandrasekar 1996; Zrnic and Ryzhkov 1999). Therefore, negative K_{DP} is a good indicator of strong electrical activity within the storm. As

Corresponding author address: Alexander V. Ryzhkov, CIMMS/NSSL, 120 David L. Boren Blvd., Norman, OK 73072.
E-mail: Alexander.Ryzhkov@noaa.gov

DOI: 10.1175/JTECH2034.1

© 2007 American Meteorological Society

opposed to K_{DP}, the corresponding differential reflectivity Z_{DR} most often remains positive because it is heavily weighted by larger size aggregates that do not align with the electrostatic field and retain their positive intrinsic Z_{DR}; K_{DP} is more transparent to the presence of such aggregates.

The situation is quite different in the case of simultaneous transmission/reception of the orthogonally polarized H and V waves. Observations with a polarimetric prototype of the S-band Weather Surveillance Radar-1988 Doppler (WSR-88D) (KOUN) in Oklahoma reveal peculiar-looking radial signatures of Z_{DR} and Φ_{DP} commonly observed in the crystal regions of thunderstorms. Differential reflectivity can either increase or decrease with slant range in frozen parts of the clouds. As will be shown in this study, these artificial-looking radial signatures of Z_{DR} are attributed to depolarization and cross-coupling in canted crystals and might create problems in polarimetric classification of hydrometeors aloft and quantitative estimation of ice water content using polarimetric data (Vivekanandan et al. 1994, 1999; Ryzhkov et al. 1998; Zrnic and Ryzhkov 1999).

Very similar effects are observed in the C-band data collected with the Environment Canada polarimetric radar in Ontario, Canada. This radar also operates in the SHV mode. Contrary to these observations, analysis of the S-band data obtained from the National Severe Storms Laboratory (NSSL) Cimarron and National Center for Atmospheric Research (NCAR) S-band Dual Polarization Doppler Radar (S-Pol) research polarimetric radars, which utilize a traditional alternate scheme of transmission/reception, reveals no such radial Z_{DR} signatures in canted crystals. Because cross-coupling in depolarizing media is common for polarimetric radars operating in the SHV mode and because this mode is the choice for the imminent upgrade of the WSR-88D network, this issue should be well understood and addressed.

The paper presents examples of strong depolarization in oriented crystals from the data collected by the polarimetric prototype of the WSR-88D radar and a theoretical model that explains the results of measurements. It is shown that the sign and magnitude of the Z_{DR} and Φ_{DP} signatures strongly depend on the orien-

→

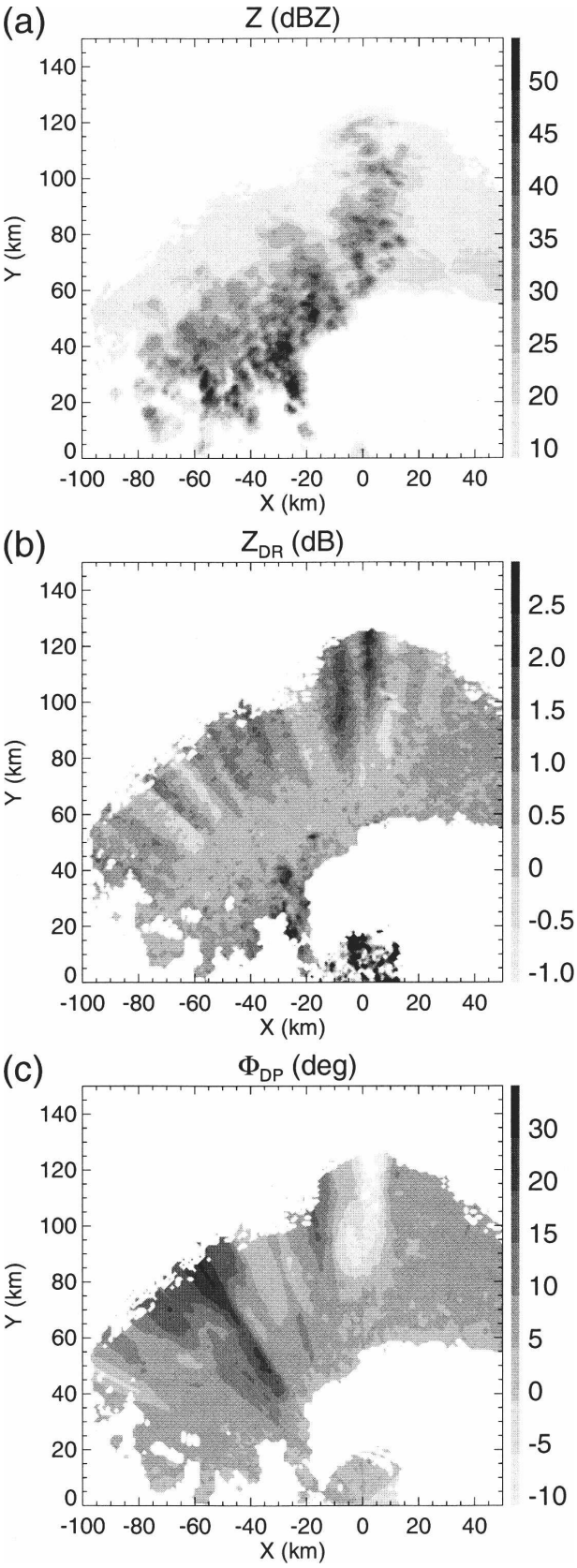

FIG. 1. A composite plan position indicator (PPI) plot of radar reflectivity Z, differential reflectivity Z_{DR}, and differential phase Φ_{DP} for the MCS observed with the KOUN radar in Oklahoma at 0906 UTC 21 Jun 2004; El = 5.5°. Simultaneous transmission/reception.

tation of crystals and the differential phase of the transmitted wave.

2. Cross-coupling polarimetric signatures

Most frequently, cross-coupling polarimetric signatures are observed in deep convective and stratiform clouds associated with warm-season mesoscale convective systems (MCSs). Two ingredients are necessary for the signature to exist: abundance of pristine, low-inertia crystals and sufficiently strong electrostatic field to orient such crystals.

A composite plot of radar reflectivity factor Z, differential reflectivity Z_{DR}, and differential phase Φ_{DP} at elevation 5.5° for the mesoscale convective system on 21 June 2004 is shown in Fig. 1. Numerous radial streaks of positive and negative Z_{DR} are evident in the crystal region of the cloud. These streaks are unlikely to be caused by differential attenuation in underlying liquid and mixed-phase hydrometeors because (i) Z_{DR} was corrected for differential attenuation, and (ii) if this were the case, then the Z_{DR} radial features would be observed at closer slant ranges, where dry aggregated snowflakes are dominant scatterers.

More detailed analysis of radial profiles of Z_{DR}, Φ_{DP}, and radar reflectivity factor at horizontal polarization Z indicates that the steepest slopes in the Z_{DR} range dependencies are associated with Z between 20 and 35 dBZ and with shallow local minima of Φ_{DP} (Fig. 2). Figure 2 exhibits strong azimuthal variability of the Z_{DR} range profiles within a relatively narrow azimuthal sector.

Radially elongated features in Z_{DR} are also clearly evident in a vertical cross section through another MCS observed with the KOUN radar on 17 June 2005 (Fig. 3). Most of those in this and similar cases originate at the tops of convective cells, and the heights usually exceed 7–8 km. Such a localization and obvious association with the areas of negative K_{DP} point to depolarization in canted crystals as a most likely cause of the signature. In the next section, we present a relatively simple theoretical model that provides physical explanation of the Z_{DR} signature and its relation to cross-coupling resulting from the use of the SHV scheme as opposed to the alternate transmission and reception of orthogonally polarized waves.

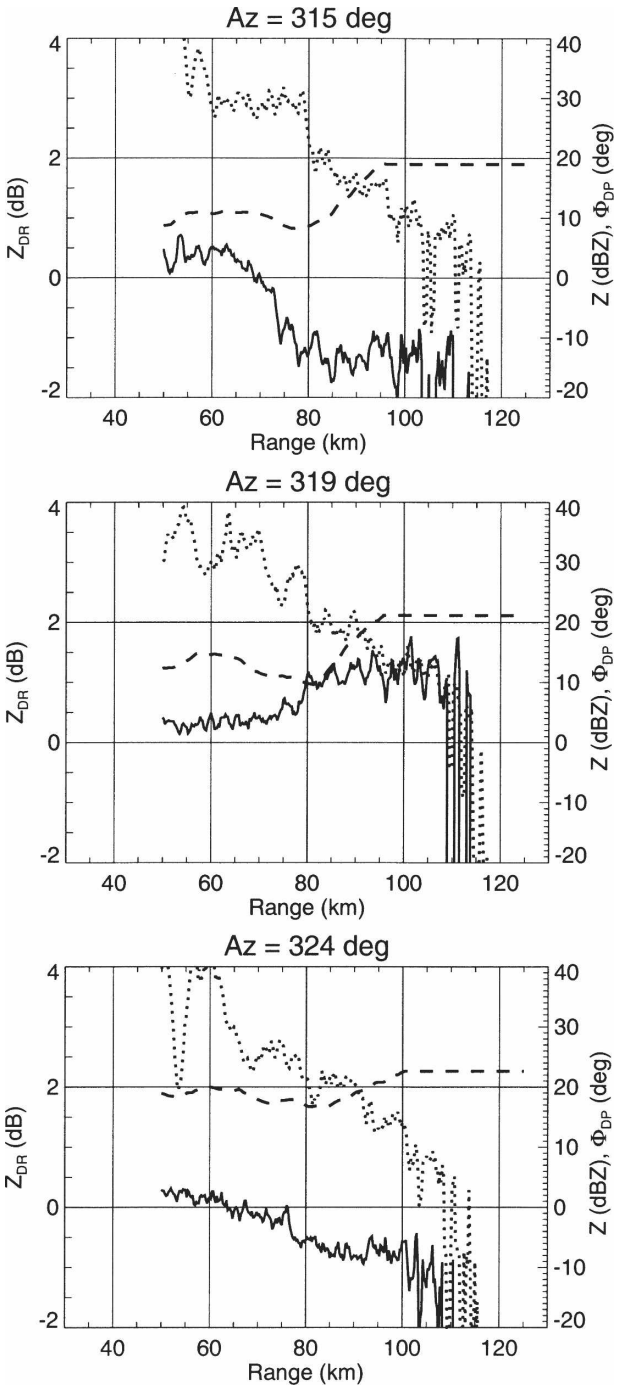

FIG. 2. Radial dependencies of Z_{DR} (solid lines), Φ_{DP} (dashed lines), and Z (dotted lines) at three azimuthal directions and elevation 5.5° for the PPI presented in Fig. 1.

3. Theoretical analysis: General formulas

Doviak et al. (2000) justified the use of a simultaneous transmission/reception (SHV) scheme for polarimetric upgrade of S-band WSR-88D radars. One of the concerns regarding the SHV scheme is inherent coupling of the H and V waves. The voltage vectors of the transmitted ($\mathbf{V}^t$) and received ($\mathbf{V}$) waves are related as

$$\mathbf{V} = C\mathbf{S}'\mathbf{V}^t, \tag{1}$$

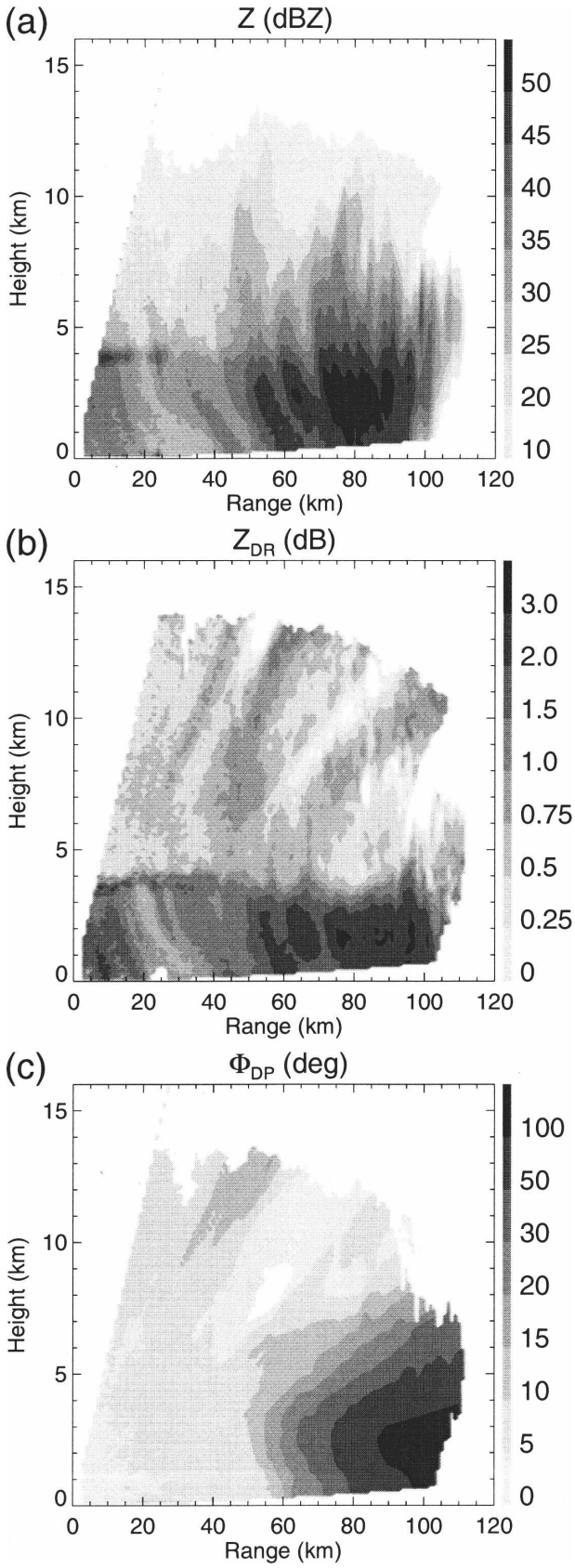

where

$$\mathbf{S}' = \mathbf{T}^{\mathrm{T}}\mathbf{S}\mathbf{T}; \tag{2}$$

C is a constant depending on the radar parameters and the distance between the radar and scatterers, $\mathbf{S}$ is the backscattering matrix representing properties of the scatterers in the radar resolution volume, and $\mathbf{T}$ is a transmission matrix describing changes in the polarization state of the EM wave as it propagates in the anisotropic medium. These changes include attenuation, differential attenuation, differential phase shift, and depolarization along propagation path. The superscript T in (2) means transposition.

In the case of alternate transmission/reception $\mathbf{V}^t = (1, 0)$ if the H wave is transmitted and $\mathbf{V}^t = (0, 1)$ if the V wave is transmitted, whereas in the SHV mode

$$\mathbf{V}^t = (e^{-j\Phi_t}, 1), \tag{3}$$

where Φ_t is a system differential phase upon transmission.

If only the H wave is transmitted, then

$$V_{\mathrm{h}} = CS'_{\mathrm{hh}}. \tag{4}$$

If only the V wave is transmitted, then

$$V_{\mathrm{v}} = CS'_{\mathrm{vv}}. \tag{5}$$

If both the H and V waves are transmitted simultaneously and the H wave acquires additional differential phase Φ_r upon reception, then

$$V_{\mathrm{h}} = Ce^{-j\Phi_r}(S'_{\mathrm{hh}}e^{-j\Phi_t} + S'_{\mathrm{hv}}) \tag{6}$$

and

$$V_{\mathrm{v}} = C(S'_{\mathrm{vv}} + S'_{\mathrm{hv}}e^{-j\Phi_t}). \tag{7}$$

The terms proportional to S'_{hv} in (6) and (7) are caused by cross-coupling between H and V waves. In Eqs. (6) and (7), it is taken into account that nondiagonal elements of the matrix $\mathbf{S}'$ are equal ($S'_{\mathrm{hv}} = S'_{\mathrm{vh}}$). These elements describe depolarizing properties of the medium. Depolarization of the backscattered H and V waves is relatively low in rain and dry aggregated snow and is significantly higher in hail and wet snow. If the mean canting angle of hydrometeors within the radar resolution volume is different from 0 or $\pm\pi/2$, then both H and V waves depolarize on propagation; that is,

←

FIG. 3. A composite range–height indicator (RHI) plot of radar reflectivity Z, differential reflectivity Z_{DR}, and differential phase Φ_{DP} for the MCS observed with the KOUN radar in Oklahoma at 0609 UTC 17 Jun 2004; Az = 191°. Simultaneous transmission/reception.

their polarization state changes from H or V as they propagate through the medium. The canting angle is determined as the angle between the direction of the axis of rotation and the projection of the vertical onto the polarization plane.

In this study, we assume that depolarization on propagation occurs only in oriented crystals because of their nonzero mean canting angle and ignore much smaller depolarization on propagation in other hydrometeor types, such as rain, graupel, hail, and wet/dry aggregated snow. Consequently, we divide the wave propagation path into depolarizing and nondepolarizing parts (with respect to propagation) and express the transmission matrix $\mathbf{T}$ as a product of the matrix $\mathbf{T}_{cr}$, describing propagation in crystals and matrix $\mathbf{T}_{nc}$ that is attributed to the rest of the propagation path. As a result, the matrix $\mathbf{S}'$ can be written as

$$\mathbf{S}' = \mathbf{T}^{T}\mathbf{S}\mathbf{T} = \mathbf{T}_{nc}^{T}\mathbf{T}_{cr}^{T}\mathbf{S}\mathbf{T}_{cr}\mathbf{T}_{nc} = \mathbf{T}_{nc}^{T}\mathbf{S}''\mathbf{T}_{nc}, \tag{8}$$

where

$$\mathbf{S}'' = \mathbf{T}_{cr}^{T}\mathbf{S}\mathbf{T}_{cr}. \tag{9}$$

The matrix $\mathbf{T}_{nc}$ in nondepolarizing medium has a simple form:

$$\mathbf{T}_{nc} = \begin{pmatrix} T_h & 0 \\ 0 & T_v \end{pmatrix}, \tag{10}$$

where

$$T_h = \exp(-j\Phi_h - \Gamma_h), \tag{11}$$

and

$$T_v = \exp(-j\Phi_v - \Gamma_v), \tag{12}$$

where $\Phi_{h,v}$ is phase shift and $\Gamma_{h,v}$ is attenuation referred to the nondepolarizing part of the propagation path. Differential phase Φ_{dp} is defined as

$$\Phi_{dp} = 2(\Phi_h - \Phi_v). \tag{13}$$

Throughout this paper, we distinguish between differential phase Φ_{dp} (lowercase subscript) associated with the nondepolarizing part of the propagation path and the measured total differential phase Φ_{DP} (uppercase subscript). Note that Φ_{dp} is caused by propagation in hydrometeors, whereas the differential phase on reception Φ_r in (6) is generated within the radar system.

Substituting (8) and (10) into (6) and (7), we obtain

$$V_h = CT_v^2\xi e^{-j(\Phi_r + \Phi_{dp}/2)}[\xi e^{-j(\Phi_t + \Phi_{dp}/2)}S''_{hh} + S''_{hv}] \tag{14}$$

and

$$V_v = CT_v^2[S''_{vv} + \xi e^{-j(\Phi_t + \Phi_{dp}/2)}S''_{hv}], \tag{15}$$

where

$$\xi = |T_h/T_v| = \exp(-\Gamma_h + \Gamma_v). \tag{16}$$

The measured differential reflectivity in the SHV mode of operation $Z_{dr}^{(s)}$ can be expressed as

$$Z_{dr}^{(s)} = \frac{\overline{|V_h|^2}}{\overline{|V_v|^2}} = \xi^4 \frac{W_{hhhh} + \xi^{-2}W_{hvhv} + 2\xi^{-1}\,\mathrm{Re}(e^{j\Psi}W_{hhhv})}{W_{vvvv} + \xi^2 W_{hvhv} + 2\xi\,\mathrm{Re}(e^{-j\Psi}W_{vvhv})}. \tag{17}$$

The measured differential phase in the SHV mode $\Phi_{DP}^{(s)}$ is given by

$$\Phi_{DP}^{(s)} = \arg(\overline{V_h^* V_v}) = \Phi_{DP}^{(sys)} + \Phi_{dp} + \arg[W_{hhvv} + e^{-j2\Psi}W_{hvhv} + e^{-j\Psi}(\xi W_{hhhv} + \xi^{-1}W_{vvhv})]. \tag{18}$$

In (17) and (18),

$$W_{hhhh} = \langle |S''_{hh}|^2\rangle,\ W_{vvvv} = \langle |S''_{vv}|^2\rangle,\ W_{hvhv} = \langle |S''_{hv}|^2\rangle,\ W_{hhvv} = \langle (S''_{hh})^* S''_{vv}\rangle,$$

$$W_{hhhv} = \langle (S''_{hh})^* S''_{hv}\rangle,\ W_{vvhv} = \langle (S''_{vv})^* S''_{hv}\rangle, \tag{19}$$

and

$$\Phi_{DP}^{(sys)} = \Phi_t + \Phi_r, \quad \Psi = \Phi_t + \Phi_{dp}/2W. \tag{20}$$

Overbars in (17) and (18) mean expected values, and angle brackets in (19) stand for ensemble averaging. In our notations, Z_{dr} (lowercase subscript) and Z_{DR} (uppercase subscript) mean differential reflectivity in linear and logarithmic scale, respectively.

According to (9), the elements of matrix $\mathbf{S}''$ can be expressed via elements of the matrix $\mathbf{S}$ and matrix

$$\mathbf{T}_{cr} = \begin{pmatrix} T_{hh} & T_{hv} \\ T_{vh} & T_{vv} \end{pmatrix} \tag{21}$$

as

$$\begin{aligned} S''_{hh} &= S_{hh}T_{hh}^2 + 2S_{hv}T_{hh}T_{vh} + S_{vv}T_{vh}^2 \\ S''_{hv} &= S''_{vh} = S_{hh}T_{hh}T_{hv} + S_{hv}(T_{hh}T_{vv} + T_{hv}T_{vh}) + S_{vv}T_{vv}T_{vh} \\ S''_{vv} &= S_{hh}T_{hv}^2 + 2S_{hv}T_{vv}T_{hv} + S_{vv}T_{vv}^2, \end{aligned} \tag{22}$$

and, correspondingly, the moments W can be expressed via elements of the matrix $\mathbf{T}_{\rm cr}$ and second-order moments of the intrinsic backscattering matrix $\mathbf{S}$.

In the alternate mode of operation, the expressions (4) and (5) for voltages $V_{\rm h}$ and $V_{\rm v}$ do not contain cross-coupling terms proportional to $S'_{\rm hv}$, and the measured differential reflectivity $Z_{\rm dr}^{(a)}$ and differential phase $\Phi_{\rm DP}^{(a)}$ are given by simpler formulas

$$Z_{\rm dr}^{(a)} = \xi^4 \frac{W_{\rm hhhh}}{W_{\rm vvvv}} \quad \text{and} \quad \Phi_{\rm DP}^{(a)} = \Phi_{\rm DP}^{(\rm sys)} + \Phi_{\rm dp} + \arg(W_{\rm hhvv}). \tag{23}$$

It is important that, contrary to the SHV scheme, the value of $Z_{\rm dr}$ measured in the alternate mode does not depend on the system differential phase upon transmission Φ_t.

4. Model simulations: Special cases

a. Oriented crystals: Constant canting angle

In a simplest case, we model scatterers as snow crystals with the same size, shape, orientation, and refractive index. It is assumed that crystals have spheroidal shape with axes a and b, where a is the axis of rotation or symmetry. Hence, $a < b$ for oblates and $a > b$ for prolates. All crystals are equioriented in the polarization plane with the canting angle α. For the sake of simplicity, we assume that the angle between the axis of rotation and the propagation vector is equal to $\pi/2$. The corresponding intrinsic backscattering matrix $\mathbf{S}$ has the form (Ryzhkov 2001)

$$\mathbf{S} = jkN\begin{bmatrix} f_b\cos^2\alpha + f_a\sin^2\alpha & (f_a - f_b)\sin\alpha\cos\alpha \\ (f_a - f_b)\sin\alpha\cos\alpha & f_b\sin^2\alpha + f_a\cos^2\alpha \end{bmatrix}, \tag{24}$$

where f_a is the scattering amplitude of individual crystals if the electric field of incident EM wave is parallel to its symmetry axis, f_b stands for the scattering amplitude if the electric vector is perpendicular to the symmetry axis, $k = 2\pi/\lambda$ is the wavenumber, and N is the number of crystals in the radar resolution volume. The transmission matrix $\mathbf{T}_{\rm cr}$ in canted crystals has a simple form for uniform propagation path (Ryzhkov 2001):

$$\mathbf{T}_{\rm cr} = \begin{pmatrix} d_b\cos^2\alpha + d_a\sin^2\alpha & (d_a - d_b)\sin\alpha\cos\alpha \\ (d_a - d_b)\sin\alpha\cos\alpha & d_b\sin^2\alpha + d_a\cos^2\alpha \end{pmatrix}. \tag{25}$$

In (25), $d_{a,b} = \exp(-j\Phi_{a,b})$ are propagation factors in the two orthogonal principal planes along the axes of spheroids. The difference,

$$\phi_{\rm dp} = 2(\Phi_a - \Phi_b) = \pm 2\int_{r_1}^{r_2} K_{\rm dp}\, dr, \tag{26}$$

characterizes intrinsic differential phase in crystals, where the plus sign in (26) corresponds to prolate scatterers because their rotation axis is the major axis of spheroid ($\Phi_a > \Phi_b$), and the minus sign corresponds to oblate scatterers for which the rotation axis is a minor one ($\Phi_a < \Phi_b$). In (26), intrinsic specific differential phase $K_{\rm dp}$ is determined in such a way that it depends on ice water content (IWC) and the shape of crystals (Vivekanandan et al. 1994; Ryzhkov et al. 1998) but not on their canting angle. The measured value of specific differential phase ($K_{\rm DP}$ with uppercase subscript) in the horizontal–vertical polarization basis is equal to $K_{\rm dp}$ only if $\alpha = \pi/2$ in the case of prolate crystals and $\alpha = 0$ in the case of oblate crystals, that is, if the larger axis of the crystal is oriented horizontally.

It can be shown that the matrix $\mathbf{S}'' = \mathbf{T}_{\rm cr}^{\rm T}\mathbf{S}\,\mathbf{T}_{\rm cr}$ can be written as (Holt 1984; Torlaschi and Holt 1993, 1998; Ryzhkov 2001)

$$\mathbf{S}'' = jkN\begin{bmatrix} f_b e^{-j2\Phi_b}\cos^2\alpha + f_a e^{-j2\Phi_a}\sin^2\alpha & (f_a e^{-j2\Phi_a} - f_b e^{-j2\Phi_b})\sin\alpha\cos\alpha \\ (f_a e^{-j2\Phi_a} - f_b e^{-j2\Phi_b})\sin\alpha\cos\alpha & f_b e^{-j2\Phi_b}\sin^2\alpha + f_a e^{-j2\Phi_a}\cos^2\alpha \end{bmatrix}. \tag{27}$$

According to (19) and substituting (26) and (27), the moments W are obtained as

$$W_{\rm hhhh} \approx k^2N[(f_b\cos^2\alpha + f_a\sin^2\alpha)^2 - f_af_b\sin^2\alpha\cos^2\alpha\phi_{\rm dp}^2], \tag{28}$$

$$W_{\rm vvvv} \approx k^2N[(f_b\sin^2\alpha + f_a\cos^2\alpha)^2 - f_af_b\sin^2\alpha\cos^2\alpha\phi_{\rm dp}^2], \tag{29}$$

$$W_{\rm hhvv} \approx k^2N[f_af_b(\cos^4\alpha + \sin^4\alpha) + (f_a^2 + f_b^2)\sin^2\alpha\cos^2\alpha - jf_af_b\cos2\alpha\phi_{\rm dp}], \tag{30}$$

$$W_{\rm hhhv} \approx \frac{1}{2}k^2N\sin2\alpha(f_a^2\sin^2\alpha - f_b^2\cos^2\alpha + f_af_b\cos2\alpha - jf_af_b\phi_{\rm dp}), \tag{31}$$

$$W_{\rm vvhv} \approx \frac{1}{2}k^2N\sin2\alpha(f_a^2\cos^2\alpha - f_b^2\sin^2\alpha - f_af_b\cos2\alpha - jf_af_b\phi_{\rm dp}) \tag{32}$$

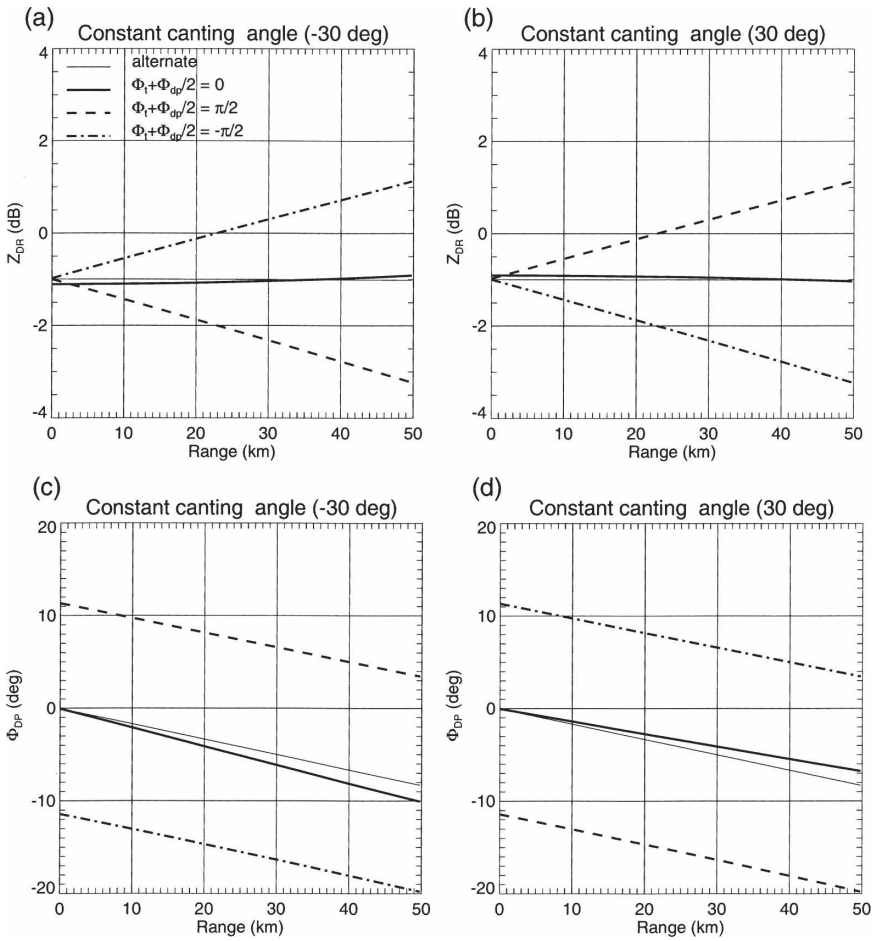

FIG. 4. Simulated radial profiles of Z_{DR} and Φ_{DP} in the cases of constant canting angle along the propagation path for different values of $\Phi_t + \Phi_{dp}/2$ for alternate transmission (thin solid lines) and simultaneous transmission (thick solid, dashed, and dot–dashed lines).

if φ_{dp} (expressed in radians) is relatively small and $\exp(\pm j\varphi_{dp}) \approx 1 \pm j\varphi_{dp}$.

Equations (28)–(32) together with Eqs. (17) and (18) were used to compute differential reflectivity and differential phase for prolate crystals with the ratio f_a/f_b equal to 1.26 so that differential reflectivity of such crystals is 2 dB if the crystals are oriented horizontally in the polarization plane. It is also assumed that K_{dp} = 1/3 IWC (Vivekanandan et al. 1994; Ryzhkov et al. 1998) and IWC = 0.5 g m^{-3}. According to formula

$$\mathrm{IWC} = 0.035Z^{0.51}, \tag{33}$$

suggested for snow by Heymsfield (1977), such a value of IWC corresponds to radar reflectivity factor of 22.6 dBZ. The results of simulations conducted for two canting angles, $-30°$ and 30°, and various values of phase Ψ are illustrated in Fig. 4. For both canting angles, vertical projection of crystals is larger than horizontal, which is often the case when crystals are oriented by a strong electric field.

In Figs. 4a,b, Z_{DR} increases or decreases with range if $\Psi \neq 0$, although orientation of crystals and their shape is uniform along the propagation path. This can be explained by the fact that depolarization in canted crystals gradually changes the polarization state of the wave as it propagates through depolarizing medium. To understand the impact of the phase Ψ on the slope of the Z_{DR} and Φ_{DP} range dependencies, we simplify Eqs. (17) and (18) by assuming no differential attenuation ($\xi = 1$) and neglecting much smaller moments W_{hvhv}:

$$Z_{dr}^{(s)} \approx \frac{W_{hhhh} + 2\cos\Psi\,\mathrm{Re}(W_{hhhv}) - 2\sin\Psi\,\mathrm{Im}(W_{hhhv})}{W_{vvvv} + 2\cos\Psi\,\mathrm{Re}(W_{vvhv}) + 2\sin\Psi\,\mathrm{Im}(W_{vvhv})} \tag{34}$$

and

$$\Phi_{\mathrm{DP}}^{(s)} \approx \Phi_{\mathrm{DP}}^{(\mathrm{sys})} + \Phi_{\mathrm{dp}} + \arg[W_{\mathrm{hhvv}} + e^{-j\Psi}(W_{\mathrm{hhhv}} + W_{\mathrm{vvhv}}^{*})]. \tag{35}$$

It follows from (28)–(32) that the moments W_{hhhh} and W_{vvvv} only weakly depend on φ_{dp} (and, consequently, range), and real parts of the moments W_{hhhv} and W_{vvhv} are not affected by φ_{dp} at all. In contrast, imaginary parts of W_{hhhv} and W_{vvhv} linearly depend on φ_{dp} [Eqs. (31) and (32)]. As a result, $Z_{\mathrm{dr}}^{(a)}$ in (23) is almost insensitive to φ_{dp} and range for a fixed canting angle (thin solid lines in Figs. 4a,b). The same is true for $Z_{\mathrm{dr}}^{(s)}$, provided that $\sin\Psi = 0$ in Eq. (34) (thick solid lines in Figs. 4a,b). However, the situation is dramatically different if $\sin\Psi \neq 0$ (dashed and dash–dot lines in Figs. 4a,b). Depending on α and Ψ, $Z_{\mathrm{dr}}^{(s)}$ either increases or decreases with range. Indeed, it follows from (31) and (32) that

$$\sin\Psi\ \mathrm{Im}(W_{\mathrm{hhhv}}) \approx \sin\Psi\ \mathrm{Im}(W_{\mathrm{vvhv}}) \propto -\sin\Psi\ \sin 2\alpha\phi_{\mathrm{dp}}, \tag{36}$$

and, according to (34), $Z_{\mathrm{dr}}^{(s)}$ increases with φ_{dp} (or with range) if $\sin\Psi\ \sin 2\alpha > 0$ and decreases with range if $\sin\Psi\ \sin 2\alpha < 0$. The largest change of $Z_{\mathrm{dr}}^{(s)}$ with range occurs if $\Psi = \pm\pi/2$.

Unlike $Z_{\mathrm{dr}}^{(s)}$, differential phase $\Phi_{\mathrm{DP}}^{(s)}$ decreases with range with almost the same slope (Figs. 4c,d), regardless of the value of Ψ and the sign of the canting angle α. Indeed, since the sum

$$W_{\mathrm{hhhv}} + W_{\mathrm{vvhv}}^{*} = \frac{1}{2}k^2 N \sin 2\alpha(f_a^2 - f_b^2) \tag{37}$$

in (35) does not depend on range, the term $e^{-j\Psi}(W_{\mathrm{hhhv}} + W_{\mathrm{vvhv}}^{*})$ in (35) generated by cross-coupling has very little impact on the slope of $\Phi_{\mathrm{DP}}^{(s)}$, which is almost entirely determined by $\arg(W_{\mathrm{hhvv}})$, that is, by the canting angle α according to (30).

b. Oriented crystals: Variable canting angle

A model with constant canting angle can explain positive and negative trends in differential reflectivity as a function of range for the fixed value of the phase Ψ as observed in the KOUN data. A more complex model with varying canting angle along the propagation path better reproduces measured radial profiles of Z_{DR} and Φ_{DP} (shown in Fig. 2). As in the previous model, canting angle is equal to either $-30°$ or $30°$, but only in the limited range interval between 7 and 33 km, whereas prolate crystals are oriented horizontally at ranges less than 3 km and larger than 37 km (Fig. 5). We also assume that equioriented crystals coexist with polarimetrically isotropic snow aggregates with a reflectivity that is 10 dB larger than that of crystals. Concentrations and sizes of both snow species are set to be constant along the propagation path.

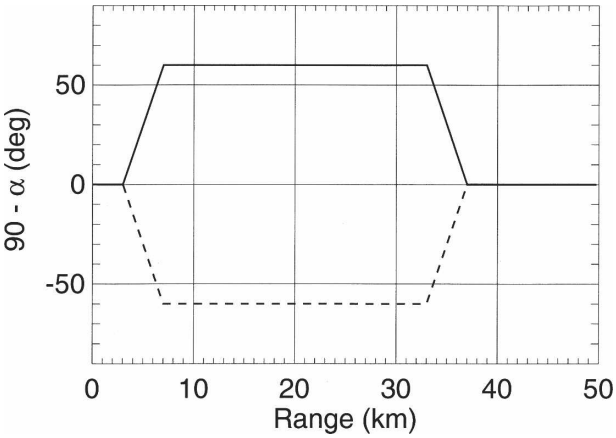

FIG. 5. Two models of the canting angle varying with range used in simulations.

In the case of varying canting angle, the simplified Eqs. (27)–(32) are not valid, and the more general Eqs. (21) and (22) should be used. The transmission matrix $\mathbf{T}_{\mathrm{cr}}$ for nonuniform propagation path with varying canting angle α can be constructed as a product of transmission matrices corresponding to short range intervals within which propagation medium can be considered uniform:

$$\mathbf{T}_{\mathrm{cr}} = \prod_{n=1}^{N} \mathbf{T}_n. \tag{38}$$

For each range interval Δr,

$$\mathrm{T}_n = \begin{pmatrix} T_{\mathrm{hh}}^{(n)} & T_{\mathrm{hv}}^{(n)} \\ T_{\mathrm{vh}}^{(n)} & T_{\mathrm{vv}}^{(n)} \end{pmatrix} = \begin{bmatrix} d_b \cos^2\alpha_n + d_a \sin^2\alpha_n & (d_a - d_b)\sin\alpha_n \cos\alpha_n \\ (d_a - d_b)\sin\alpha_n \cos\alpha_n & d_b \sin^2\alpha_n + d_a \cos^2\alpha_n \end{bmatrix}, \tag{39}$$

where α_n is a canting angle in the nth interval,

$$d_{a,b} = \exp(-j\gamma_{a,b}\Delta r), \tag{40}$$

and $\gamma_a - \gamma_b = \pm K_{\mathrm{dp}}$, where intrinsic K_{dp} is defined in the previous subsection. Because isotropic snow aggregates do not produce differential phase shift, the magnitude of K_{dp} is entirely determined by IWC and shape of crystals. We assume the same uniform shape and IWC of crystals along the propagation path as in the previous subsection. Only crystal orientation varies.

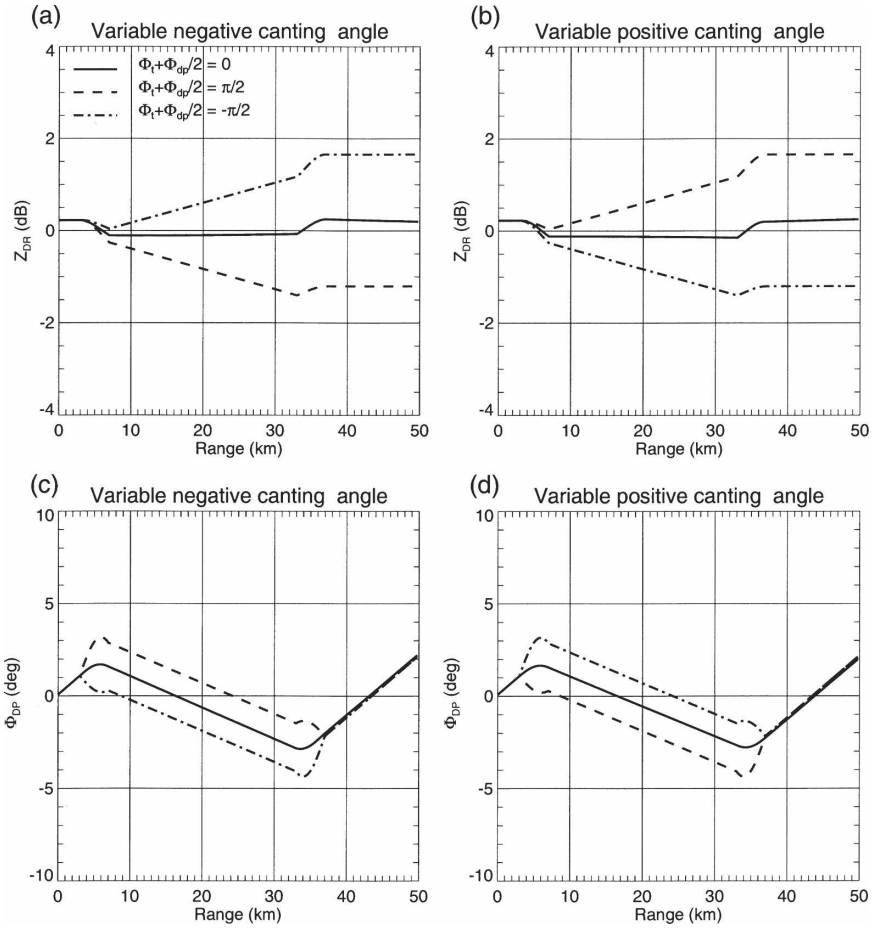

FIG. 6. Simulated radial profiles of Z_{DR} and Φ_{DP} in the cases of variable canting angle along the propagation path for different values of $\Phi_t + \Phi_{dp}/2$ for simultaneous transmission/reception. The models of variable canting angle are illustrated in Fig. 5.

Results of numerical simulations for varying canting angle are displayed in Fig. 6. Due to the substantial presence of polarimetrically isotropic snow aggregates mixed with crystals, the "background" value of Z_{DR} (if crystals are not canted) does not differ from zero by more than 0.25 dB, although the intrinsic value of Z_{DR} for horizontally oriented crystals is 2 dB. As in the case of the pure crystals examined in the previous subsection, depolarization effects due to canting cause substantial decrease or increase of $Z_{DR}^{(s)}$ in the range interval where canting occurs (Figs. 6a,b). The sign and magnitude of this trend depends on the canting angle α and the phase Ψ. It is important that, at ranges beyond 37 km, where crystals are not canted, the absolute value of Z_{DR} remains high compared to its background value if $\Psi = \pm\pi/2$. This explains the "radial streak" appearance of the Z_{DR} signatures in Figs. 1 and 3.

Simulated radial dependencies of $Z_{DR}^{(s)}$ and $\Phi_{DP}^{(s)}$ in Fig. 6 adequately reproduce the measured radial profiles of Z_{DR} and Φ_{DP} presented in Fig. 2. Note that nonmonotonic range dependence of differential phase in Fig. 2 is also explained by the model. A slope of the radial profile of Φ_{DP} in the region of canted crystals depends primarily on the canting angle: it is negative if $|\alpha| < \pi/4$ and positive if $|\alpha| > \pi/4$. In contrast, a slope of the radial profile of Z_{DR} is determined by both canting angle and the phase Ψ. It is positive if $\alpha > 0$ and $\Psi > 0$ or $\alpha < 0$ and $\Psi < 0$. The slope is negative if $\alpha > 0$ and $\Psi < 0$ or $\alpha < 0$ and $\Psi > 0$.

5. Discussion and summary

Model simulations in the previous section demonstrate that spurious radial Z_{DR} signatures are attributed to depolarization in canted crystals. Depolarization produces a cross-polar backscatter component and gradually changes the polarization state of the propa-

gating wave. Traditionally a degree of depolarization is measured by linear depolarization ratio (LDR) and cross-polar correlation coefficients ρ_{xh} and ρ_{xv} defined as (Ryzhkov et al. 2002)

$$\mathrm{LDR} = \frac{W_{hvhv}}{\xi^2 W_{hhhh}}, \rho_{xh} = \frac{W_{hhhv}}{(W_{hhhh}W_{hvhv})^{1/2}}, \quad \text{and} \quad \rho_{xv} = \frac{W_{vvhv}}{(W_{vvvv}W_{hvhv})^{1/2}}, \tag{41}$$

where the moments W are specified in Eq. (19). As was shown by Ryzhkov (2001),

$$\rho_{xh,xv} \propto \frac{\sin 2\langle\alpha\rangle}{\sigma_\alpha}, \tag{42}$$

where $\langle\alpha\rangle$ is the mean canting angle and σ_α is the rms width of the canting angle distribution. Neither LDR nor ρ_{xh} and ρ_{xv} are measured in the SHV mode. They, however, indirectly affect $Z_{dr}^{(s)}$ and $\Phi_{DP}^{(s)}$ measured in the SHV mode via cross-coupling terms proportional to W_{hhhv}, W_{vvhv}, and W_{hvhv} in Eqs. (17), (18), (34), and (35).

Figure 7 illustrates vertical cross sections of LDR, ρ_{xh}, and ρ_{xv}, as well as Z, Z_{DR}, and K_{DP} in the thunderstorm cloud observed with the NCAR S-Pol radar in Florida. This case was examined in more detail in Ryzhkov et al. (2002). Radial streaks of high LDR, ρ_{xh}, and ρ_{xv} at a height exceeding 8 km manifest strong depolarization due to crystal canting. It is very likely that actual crystal canting occurs in a relatively small area next to the top of the reflectivity core. Once the propagating wave changes its polarization state due to depolarization, LDR, ρ_{xh}, and ρ_{xv} remain high along the rest of the ray regardless of crystal orientation. According to (34), these high values of LDR, ρ_{xh}, and ρ_{xv} (or W_{hvhv}, W_{hhhv}, and W_{vvhv}, respectively) would have been associated with Z_{DR} streaks because of cross-coupling if the S-Pol radar were operating in the SHV mode. In fact, the S-Pol radar utilized an alternate transmission/reception scheme, and the Z_{DR} field in Fig. 7 is streak-free.

This proves that, in full agreement with Eq. (23), Z_{DR} is not affected by cross-coupling in the case of alternate transmission and reception. The situation is quite different in the SHV mode of operation. In the latter case, the Z_{DR} signature depends on the phase Ψ, which is a sum of the system differential phase on transmission Φ_t and differential phase $\Phi_{dp}/2$ acquired along the propagation path before the microwave radiation reaches the region of oriented crystals. If Ψ is different from zero and does not change much due to possible variations of Φ_{dp}, then the change of the sign of the Z_{DR} signature in Figs. 1 and 2 in relatively close azimuthal directions is solely attributed to the change in the sign of the canting angle.

One may think about mitigating the impact of cross-coupling on Z_{DR} and Φ_{DP} by controlling and adjusting Φ_t. As follows from Figs. 4 and 6, there is practically no difference between Z_{DR} measured in the SHV and alternate modes [$Z_{DR}^{(s)}$ and $Z_{DR}^{(a)}$] if $\Phi_t = 0$ (and $\Phi_{dp} = 0$) (i.e., the radar transmits electromagnetic wave with slanted 45° linear polarization). The largest difference between $Z_{DR}^{(s)}$ and $Z_{DR}^{(a)}$ occurs if $\Phi_t = \pm\pi/2$, (i.e., the transmitted wave has either left- or right-hand circular polarization). Then the Z_{DR} radial signatures in the SHV mode are most pronounced. This may not be a deficiency if one is interested in evaluating hydrometeor orientations or the properties of electrostatic fields in electrically charged zones in the cloud.

Differential phase on transmission Φ_t can be measured using the technique described by Zrnic et al. (2006). It requires measurements of differential phase in rain for both the SHV and alternate modes. It is useful to know Φ_t for better interpretation of the $Z_{DR}^{(s)}$ and $\Phi_{DP}^{(s)}$ fields. Phase adjustment requires a tunable phase shifter operating at high frequency, which presents a technical challenge. On the other hand, one has to keep in mind that it is possible to adjust Φ_t but not the Φ_{dp} term in the total phase Ψ. This means that making Φ_t equal to zero does not guarantee the absence of Z_{DR} streaks.

Our theoretical model and simulations show that cross-coupling terms in the expressions for Z_{DR} in the case of simultaneous transmission/reception of the H and V waves are roughly proportional to the product of $\sin(2\alpha)\varphi_{dp}$, where φ_{dp} is the differential phase increment within the region of canted crystals (Ryzhkov 2001). Because φ_{dp} is inversely proportional to the radar wavelength, then stronger coupling effects and more pronounced radial Z_{DR} signatures are expected at higher microwave frequencies.

Finally, we would like to make a comment on the relation between LDR and Z_{DR} measured in the SHV mode. There is an apparent similarity between radial signatures of Z_{DR} in Figs. 1 and 3 and LDR in Fig. 7a. Underlying reasons for the LDR and Z_{DR} signatures are the same. Both are attributed to depolarization in oriented crystals, and the radial appearance of the signatures is a result of depolarization on propagation (see also Fig. 5b of Ryzhkov 2001). The difference is that the

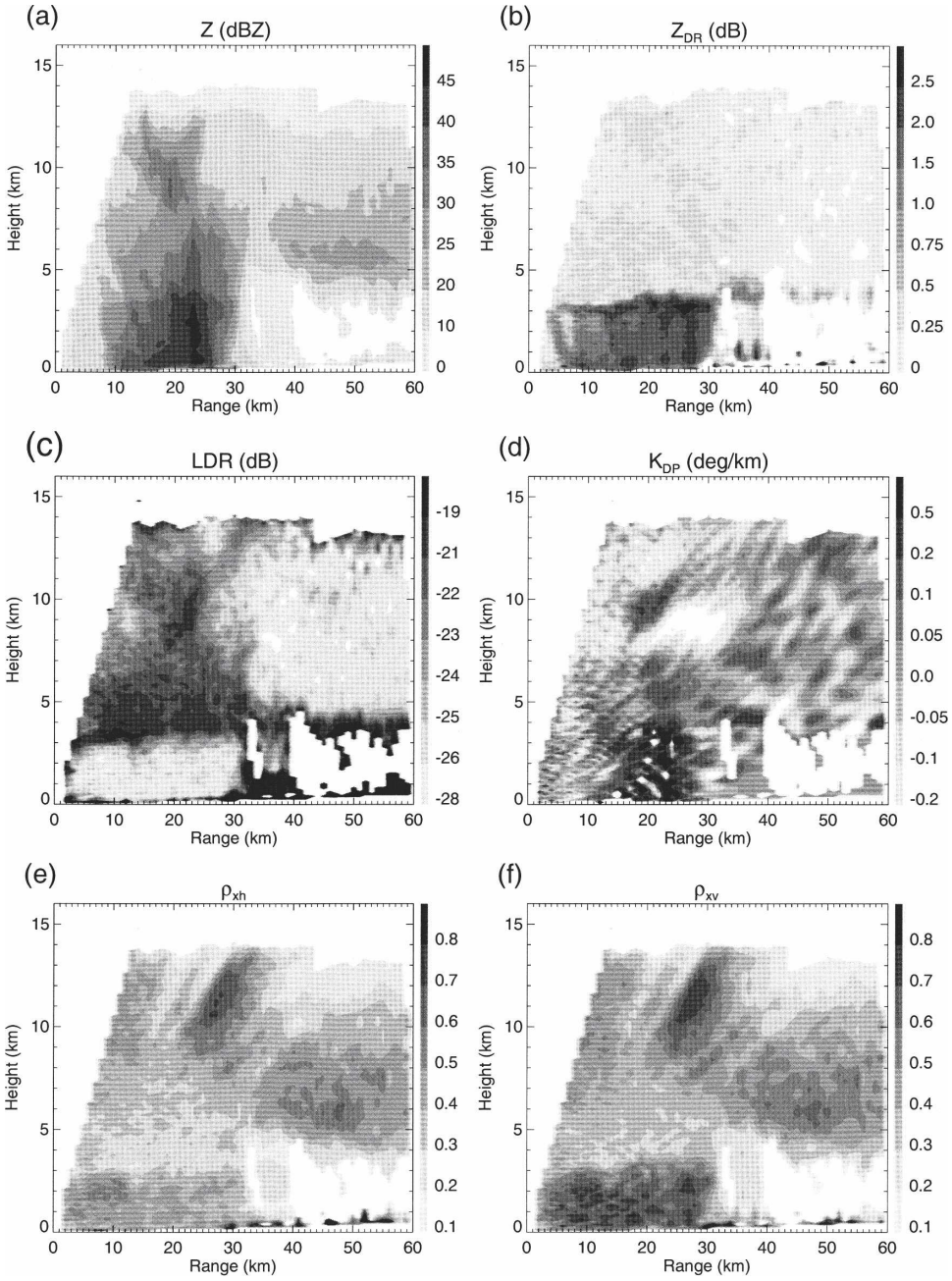

FIG. 7. A composite RHI plot of radar reflectivity Z, differential reflectivity Z_{DR}, linear depolarization ratio LDR, specific differential phase K_{DP}, and co-cross-polar correlation coefficients ρ_{xh} and ρ_{xv} for the thunderstorm observed by the NCAR S-Pol radar in Florida on 18 Aug 1998. Alternate transmission/reception.

magnitude of Z_{DR} and its radial slope depend on the absolute value and sign of the mean canting angle $\langle\alpha\rangle$ as well as on the system differential phase on transmission Φ_t, whereas LDR and its slope do not depend on the sign of $\langle\alpha\rangle$ and on Φ_t because there is no such a thing as differential phase on transmission in the LDR mode when the H and V waves are not transmitted simultaneously.

In summary, we can conclude the following.

1) Radial streaks in differential reflectivity Z_{DR} are commonly observed in the ice parts of thunderstorm

clouds if a polarimetric radar simultaneously transmits and receives horizontally and vertically polarized waves (SHV mode of operation).

2) Such Z_{DR} signatures are not observed if the orthogonally polarized waves are alternately transmitted and received.
3) Radial Z_{DR} signatures in the SHV mode are attributed to cross-coupling between orthogonally polarized waves, which is caused by depolarization in canted crystals that most likely change their orientation under the influence of strong electrostatic fields.
4) A slope of the radial profile of differential phase Φ_{DP} in the regions of aligned crystals is primarily determined by the magnitude of the canting angle, whereas the corresponding slope of Z_{DR} profile depends both on the canting angle and the value of the phase $\Psi = \Phi_t + \Phi_{dp}/2$, where Φ_t is a system differential phase on transmission and $\Phi_{dp}/2$ is an additional phase between H and V waves that is acquired while both waves travel through nonspherical hydrometeors before reaching the crystal regions.
5) The impact of cross-coupling on Z_{DR} in the SHV mode is minimal if $\Psi = 0$ and maximal if $\Psi = \pm\pi/2$. In the former case, polarization of the incident wave is linear (45° slanted), whereas in the latter case it is circular. In both the simultaneous and alternate transmission/reception modes, Z_{DR} measurements are almost identical if $\Psi = 0$.

Acknowledgments. Funding for this study was provided by the NOAA/Office of Oceanic and Atmospheric Research under NOAA–University of Oklahoma Cooperative Agreement NA17RJ1227, U.S. Department of Commerce, and from the U.S. National Weather Service, the Federal Aviation Administration (FAA), and the Air Force Weather Agency through the NEXRAD Products Improvement Program. The authors thank NCAR scientists E. Brandes, J. Vivekanandan, and R. Rilling for providing the S-Pol polarimetric data. We are grateful to Dr. V. Melnikov for reading this manuscript and for making useful comments. The support from the NSSL and CIMMS/University of Oklahoma staff who maintain and operate the KOUN WSR-88D polarimetric radar is also acknowledged.

REFERENCES

Caylor, I. J., and V. Chandrasekar, 1996: Time-varying crystal orientation in thunderstorms observed with multiparameter radar. *IEEE Trans. Geosci. Remote Sens.,* **34,** 847–858.

Doviak, R. J., V. N. Bringi, A. V. Ryzhkov, A. Zahrai, and D. S. Zrnic, 2000: Considerations for polarimetric upgrades to operational WSR-88D radars. *J. Atmos. Oceanic Technol.,* **17,** 257–278.

Hendry, A., and G. C. McCormick, 1976: Radar observations of alignment of precipitation particles by electrostatic fields in thunderstorms. *J. Geophys. Res.,* **81,** 5353–5357.

Heymsfield, A. J., 1977: Precipitation development in stratiform ice clouds: A microphysical and dynamical study. *J. Atmos. Sci.,* **34,** 367–381.

Holt, A. R., 1984: Some factors affecting the remote sensing of rain by polarization diversity radar echo characteristics. *Radio Sci.,* **22,** 37–50.

Hubbert, J. C., and V. N. Bringi, 2003: Studies of polarimetric covariance matrix. Part II: Modeling and polarization errors. *J. Atmos. Oceanic Technol.,* **20,** 1011–1022.

Krehbiel, P. R., T. Chen, S. McCrary, W. Rison, G. Gray, and M. Brook, 1996: The use of dual-channel circular-polarization radar observations for remotely sensing storm electrification. *Meteor. Atmos. Phys.,* **59,** 65–82.

Metcalf, J. I., 1997: Temporal and spatial variations of hydrometeor orientation of hydrometeors in thunderstorms. *J. Appl. Meteor.,* **36,** 315–321.

Ryzhkov, A. V., 2001: Interpretation of polarimetric radar covariance matrix for meteorological scatterers: Theoretical analysis. *J. Atmos. Oceanic Technol.,* **18,** 315–328.

——, D. S. Zrnic, and B. Gordon, 1998: Polarimetric method for ice water content determination. *J. Appl. Meteor.,* **37,** 125–134.

——, ——, J. C. Hubbert, V. N. Bringi, J. Vivekanandan, and E. A. Brandes, 2002: Polarimetric radar observations and interpretation of co-cross-polar correlation coefficients. *J. Atmos. Oceanic Technol.,* **19,** 340–354.

Scott, R. D., P. R. Krehbiel, and W. Rison, 2001: The use of simultaneous horizontal and vertical transmissions for dual-polarization radar meteorological observations. *J. Atmos. Oceanic Technol.,* **18,** 629–648.

Torlaschi, E., and A. R. Holt, 1993: Separation of propagation and backscattering effects in rain for circular polarization diversity S-band radars. *J. Atmos. Oceanic Technol.,* **10,** 465–477.

——, and ——, 1998: A comparison of different polarization schemes for the radar sensing of precipitation. *Radio Sci.,* **33,** 1335–1352.

Vivekanandan, J., V. N. Bringi, M. Hagen, and P. Meischner, 1994: Polarimetric radar studies of atmospheric ice particles. *IEEE Trans. Geosci. Remote Sens.,* **32,** 1–10.

——, D. S. Zrnic, S. M. Ellis, R. Oye, A. V. Ryzhkov, and J. Straka, 1999: Cloud microphysics retrieval using S-band dual-polarization radar measurements. *Bull. Amer. Meteor. Soc.,* **80,** 381–388.

Wang, Y., V. Chandrasekar, and V. N. Bringi, 2006: Characterization and evaluation of hybrid polarization observation of precipitation. *J. Atmos. Oceanic Technol.,* **23,** 552–572.

Zrnic, D. S., and A. V. Ryzhkov, 1999: Polarimetry for weather surveillance radars. *Bull. Amer. Meteor. Soc.,* **80,** 389–406.

——, V. M. Melnikov, and A. V. Ryzhkov, 2006: Correlation coefficients between horizontally and vertically polarized returns from ground clutter. *J. Atmos. Oceanic Technol.,* **23,** 381–394.